

# Chapter 2

## Retinal Connectomics

Kevin L. Briggman

**Abstract** The use of electron microscopy (EM) to describe the detailed synaptic connectivity in the retina has a rich history. Recent technological advances in serial electron microscopy (EM) have placed a complete description of the synaptic connectivity of the mammalian retina within reach. These new tools have recently been used to densely reconstruct the largest piece of a mammalian retina to date. Connectivity mapping has also revealed an unprecedented degree of wiring specificity in retinal circuitry. This is only the beginning of what can be learned from the comprehensive mapping of retinal circuits. The field of retinal connectomics is rapidly contributing to the functional understanding of retinal computation and enabling wiring comparisons both within and across species.

### 2.1 Introduction

The circuitry of the mammalian retina is primarily responsible for decomposing (or filtering) the visual world into a series of parallel representations (Gollisch and Meister 2010). While the purpose of these filters are intuitive to describe such as the detection of edges or motion or the adaptation to changes in color or luminance, the synaptic circuitry that underlies the majority of retinal computations remains to be discovered. In other words, we know a lot about what the retina can do, but much less about how it accomplishes specific computations. Indeed, even the absolute number of output channels in the mammalian retina—defined as distinct retinal ganglion cell (GC) types—continues to increase with each new functional or anatomical survey of cell types (Kong et al. 2005; Helmstaedter et al. 2013; Sanes and Masland 2015; Baden et al. 2016). For the few retinal circuits in which detailed synaptic wiring has been described, it is clear that circuit mapping is one essential

---

K.L. Briggman (✉)

Circuit Dynamics and Connectivity Unit, National Institute  
of Neurological Disorders and Stroke (NINDS), Bethesda  
MD 20892, USA

e-mail: kevin.briggman@nih.gov

© Springer International Publishing AG 2017

A. Çelik and M.F. Wernet (eds.), *Decoding Neural Circuit  
Structure and Function*, DOI 10.1007/978-3-319-57363-2\_2

component for understanding how functional responses in the retina arise (Briggman et al. 2011; Kim et al. 2014; Marc et al. 2014).

This chapter explores both the history of electron microscopy-based circuit mapping in the mammalian retina and the current state of large connectomic reconstruction efforts. In particular, modern electron microscopy (EM) tools and analysis algorithms have transformed the experimental landscape, enabling the collection of sufficiently large data volumes, at unprecedented spatial resolutions, to analyze complete retinal microcircuits. When combined with functional recordings from retinal neurons—ideally in the same piece of tissue—these methods now allow direct correlations between structure and function in the mammalian retina and provide crucial information for anatomically accurate computational models of retinal circuits.

## 2.2 Some Basic Retinal Anatomy

Unlike nearly all other regions of the central nervous system, the mammalian retina is essentially a standalone computational device. It consists of highly ordered layers of neuronal cell bodies [the outer and inner nuclear layers (ONL, INL) and the ganglion cell layer (GCL)] interconnected by dense synaptic neuropil layers [the outer and inner plexiform layers (OPL, IPL)] (Fig. 2.1). Five general cell classes populate the nuclear layers: photoreceptors, horizontal cells, bipolar cells (BCs), amacrine cells (ACs), and ganglion cells (GCs). The basic wiring plan of the retina was described by Dowling and Boycott by examining electron micrographs of the primate retina (Dowling and Boycott 1966). Their plan outlines a forward propagation of information from photoreceptors to ganglion cells with extensive lateral interactions implemented by horizontal and amacrine cells (Fig. 2.2a). Two ultra-structurally distinct classes of chemical synapses—ribbon synapses formed by photoreceptors and BCs, and more classical synapses formed by ACs—were also identified (Kidd 1962; Dowling and Boycott 1966) (Fig. 2.2b).

The major cell classes have been further subdivided based on distinct morphological differences and, for BCs, ACs, and GCs, stratification level within the IPL (MacNeil and Masland 1998; Masland 2012; Sanes and Masland 2015). While the diversity in cell-type morphologies was already appreciated by Cajal (Ramón y Cajal 1972) and early Golgi impregnation studies (Kolb et al. 1981), counting the actual number of subtypes has proven difficult. A historical timeline of anatomical cell-type surveys demonstrates both the upward trend in the number of defined subtypes and the increasing frequency of attempted surveys (Fig. 2.3). Part of the reason for the increased interest in defining cell types was the introduction of new experimental tools to label neuronal morphologies, including the stochastic expression of genetic reporters (Badea and Nathans 2004), photofilling (MacNeil et al. 1999), DIOListic labeling (Gan et al. 2000), and the availability of mouse lines labeling genetically distinct subtypes (Sümbül et al. 2014). Each of these methods, however, comes with intrinsic biases that influence which neurons will be labeled.

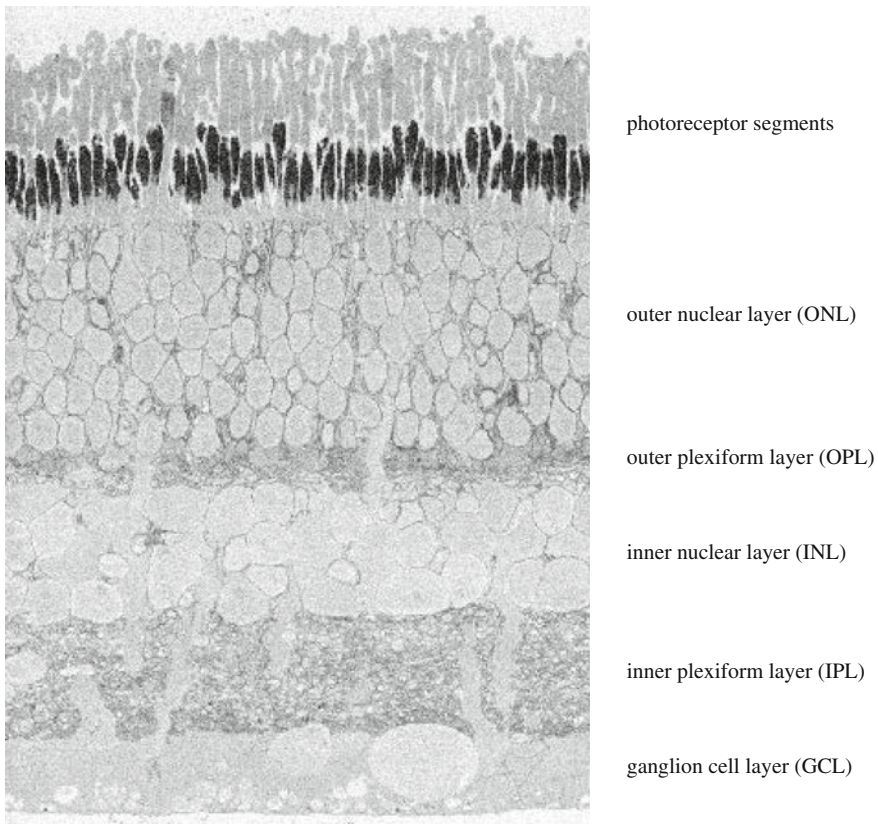


**Fig. 2.1** A low power electron micrograph of a cross section through a rabbit retina. Retinal ganglion cell somas reside in the GCL. Bipolar, amacrine, and horizontal cell somas in the INL. Rod and cone photoreceptors in the ONL. Synapses between photoreceptors and bipolar cell dendrites occur in the OPL. Synapses between bipolar cell axons, amacrine cells, and ganglion cells are found in the IPL. Scale bar 50  $\mu$ m

For example, any filling technique that depends on randomly sampling a grid placed over neuronal cell bodies will bias the filling of neurons with large somas. The only truly unbiased approach is a method in which every neuron within a given volume can be comprehensively reconstructed. This is perhaps a trivial point but one that is often underappreciated and is a clear advantage for EM-based dense volume reconstructions (Helmstaedter et al. 2013; Kasthuri et al. 2015).

As of 2016, the current cell-type counts in the mouse retina are 10 BC types, 45 AC types, and 30+ GC types (Helmstaedter et al. 2013; Sanes and Masland 2015). These numbers could easily increase as larger EM volumes become available that encompass sparse and/or large, wide-field cell types. Moreover, it is not clear how representative these numbers are for other species in which large-scale surveys have not yet been undertaken. In other words, the most basic prerequisite

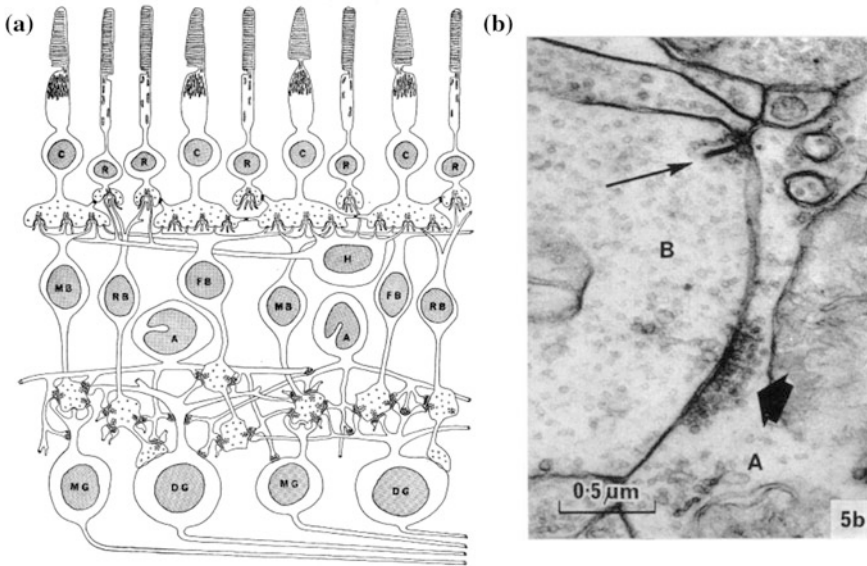


**Fig. 2.2** **a** Basic synaptic organization of the mammalian retina based on early EM reconstructions by Dowling and Boycott in the central primate retina. This classic picture of the synaptic organization of the retina has not fundamentally changed in the last 50 years. During that time period, however, the number of unique cell types has continuously risen and the complexity of the wiring diagram is still under investigation. **b** A classic example of the two types of chemical synapses encountered in the ribbon; ribbon synapses found in photoreceptors and bipolar cells and classical chemical synapses formed by amacrine cells. Reproduced from Dowling and Boycott (1966)

for mapping neuronal circuitry—knowing how many distinct cell types exist in the retina—has only very recently reached some semblance of completeness and, at that, in only one mammalian species.

### 2.3 Why Is Retinal Connectomics Difficult?

The use of EM to describe the wiring of the retina has waxed and waned since the original images of synapses acquired by Dowling and Boycott (1966). Early efforts to identify synaptic contacts onto defined cell types typically used Golgi impregnation or horseradish peroxidase (HRP) to first fill a neuron for viewing under a light microscope and then collecting small, local EM volumes around a stained dendrite (Kolb 1970). The first serious attempts to collect and annotate volumes sufficiently large to trace dendritic trees were undertaken by Peter Sterling and colleagues (Stevens et al. 1980a, b). Their data volumes were typically around

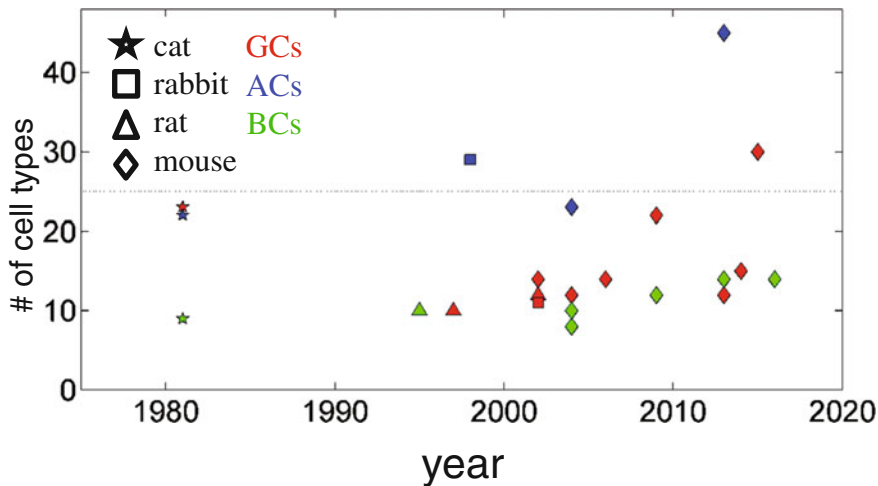


**Fig. 2.3** Historical view of the number of ganglion cell (GC), amacrine cell (AC), and bipolar cell (BC) types estimated from the cat, rabbit, rat, and mouse retinas. Early estimates were based on the stochastic Golgi method. More recent estimates used random filling of neurons with fluorescent dyes, gene expression, or dense reconstruction of SBEM datasets. Some variability is due to differences in counting conventions, but note the general upward trend and increasing frequency of estimates. Data points derived from Kolb et al. (1981), Euler and Wässle (1995), Huxlin and Goodchild (1997), MacNeil et al. (1999), Rockhill et al. (2002), Sun et al. (2002a), Sun et al. (2002b), Badea and Nathans (2004), Ghosh et al. (2004), Coombs et al. (2006), Volgyi et al. (2009), Wässle et al. (2009), Helmstaedter et al. (2013), Sümbül et al. (2014), Sanes and Masland (2015), and Greene et al. (2016)

$10^4 \mu\text{m}^3$  (Fig. 2.4) and were focused on mapping the bipolar cell input pathways to several GC types in the cat and primate retinas (Stevens et al. 1980a, b; McGuire et al. 1984; Freed and Sterling 1988; Sterling et al. 1988; Cohen and Sterling 1990; Calkins et al. 1998).

Given the importance of accurately describing cell types and mapping the connectivity among all cell types, why have large-scale efforts equivalent to the comprehensive mapping of the *C. elegans* nervous system (White et al. 1986) only recently been undertaken? What took so long? First, the necessity to manually collect and analyze thousands of sections to reconstruct a sufficiently large volume to contain complete circuits was daunting (and tedious) (Stevens et al. 1980a, b). Second, many of the neuronal structures in the retina require higher resolutions than had been achievable. The limiting resolution in serial section electron microscopy is not the imaging resolution of an electron microscope, but rather, the actual section thickness. For decades, section thicknesses of 50–80 nm were considered state-of-the-art (Fig. 2.4). Are 50–80 nm sections sufficient to unambiguously reconstruct all arbitrarily oriented thin neurites and synaptic structures in a volume? The answer is clearly no, see discussion below. Third, the computing requirements to both manage and analyze large-scale datasets have only recently become readily available (Jain et al. 2010; Turaga et al. 2010; Helmstaedter et al. 2011; Berning et al. 2015).

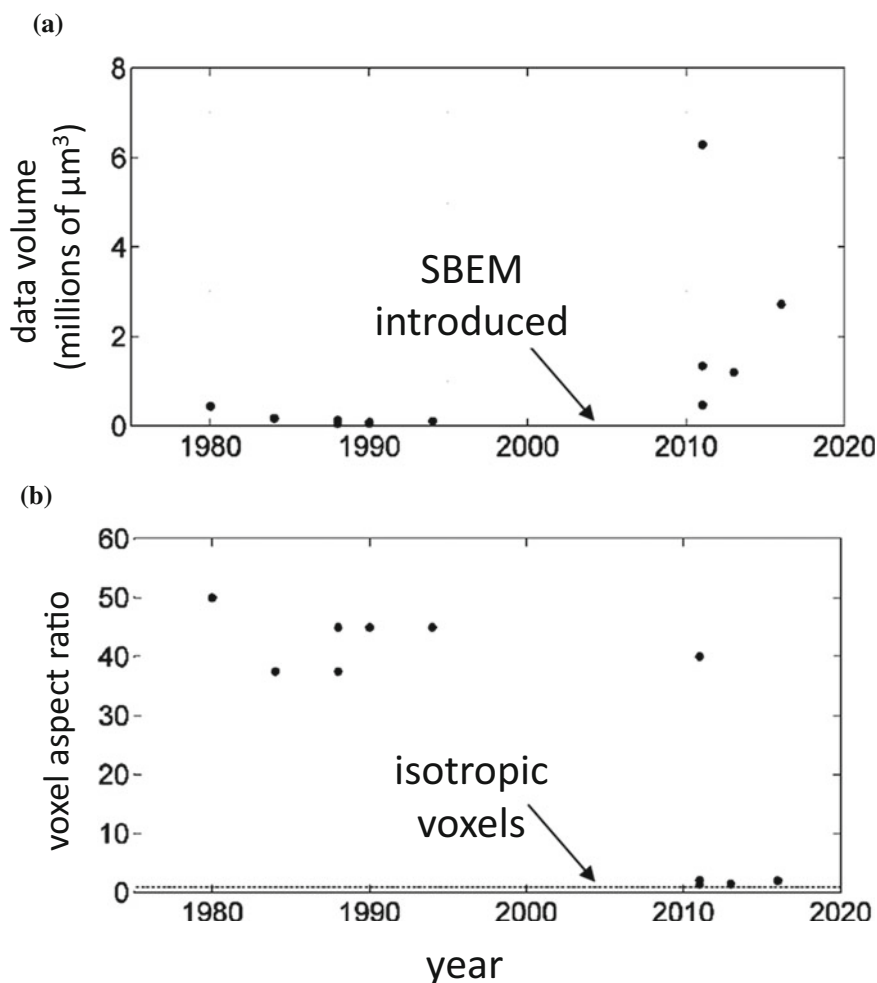


**Fig. 2.4** **a** Historical view of the volume encompassed by a selection of mammalian retina EM datasets. Studies not reporting section thicknesses and/or imaged area dimensions are not shown. Since the introduction of automated acquisition techniques, dataset volumes have grown, in one case by an order of magnitude over what was collected by ssTEM. **b** Automated sectioning methods have allowed section thicknesses to dramatically decrease from 70–90 nm to 25–30 nm. Consequently, the aspect ratio (defined as the ratio of section thickness over lateral pixel resolution) of voxels has decreased. Current methods are approaching isotropic voxel resolutions. For earlier studies that used photographic film rather than cameras, a lateral resolution of 2 nm was assumed. Data points derived from Stevens et al. (1980a, b), McGuire et al. (1984), Freed and Sterling (1988), Cohen and Sterling (1990), Strettoi et al. (1990), Calkins et al. (1998), Anderson et al. (2011), Helmstaedter et al. (2011), Helmstaedter et al. (2013), and Ding et al. (2016)

## 2.4 The Long Overdue Automation of Electron Microscopy

For decades 3D EM data, including retinal EM data, were collected by serial section transmission electron microscopy (ssTEM, Fig. 2.5a). ssTEM involves cutting ultrathin sections with an ultramicrotome and the manual collection of the sections from a water boat. This is a tedious and inherently error-prone process that can result in a number of artifacts such as lost or folded sections. The sections are then sequentially imaged with a TEM and then aligned and assembled into a 3D volume. There was remarkably little innovation in this process until the early 2000s, when two complementary approaches were introduced to automate the sectioning process. One was termed the automated tape-collecting ultramicrotome (ATUM) (Schalek et al. 2011). The idea was to remove human interaction from the collection of sections by automatically feeding sections onto a support film like a conveyor belt. The support film is subsequently cut into strips, mounted on a metal substrate and imaged in a scanning electron microscope (SEM). A second approach was named serial block-face scanning electron microscopy (SBEM) (Denk and Horstmann 2004). SBEM removes the requirement of pre-sectioning tissue by mounting a custom microtome within the vacuum chamber of a SEM. Images are formed from the block face of a sample and tissue sections are then shaved off the block face.

Both of these advances benefited from the relatively recent development of high-resolution scanning electron microscopes and efficient electron detectors. Indeed, block-face imaging had been attempted decades earlier (Leighton 1981), but did not catch on with the SEMs available at that time. The automation afforded by both ATUM and SBEM is a clear advantage when collecting tens of thousands of sections. Perhaps more important is the reduction in section thickness that automation enabled. The typical slice thickness for ssTEM is still around 50–70 nm. ssTEM voxels are therefore extremely anisotropic (assuming a lateral TEM resolution of 2 nm) (Fig. 2.4b). Even 50-nm-thick sections are clearly inadequate when the diameters of neurites approach 100 nm (of which several examples exist in the retina, such as the dendrites of starburst amacrine cells). One of the few published accounts of the difficulties encountered while tracing neurons was reported by Freed and Sterling describing their experience tracing bipolar cells using 75 nm sections: “We could not trace the processes back to an axon stalk because the connections between these varicosities were extremely fine and tortuous” (Freed and Sterling 1988). Both ATUM and SBEM allow substantially thinner sections to be reliably cut down to a range of 20–30 nm (approaching isotropic voxels, Fig. 2.4) and miss far fewer sections than ssTEM. However, even using modern automated EM approaches with section thicknesses of  $\sim 25$  nm, inter-annotator tracing discrepancies still persist (Helmstaedter et al. 2011).



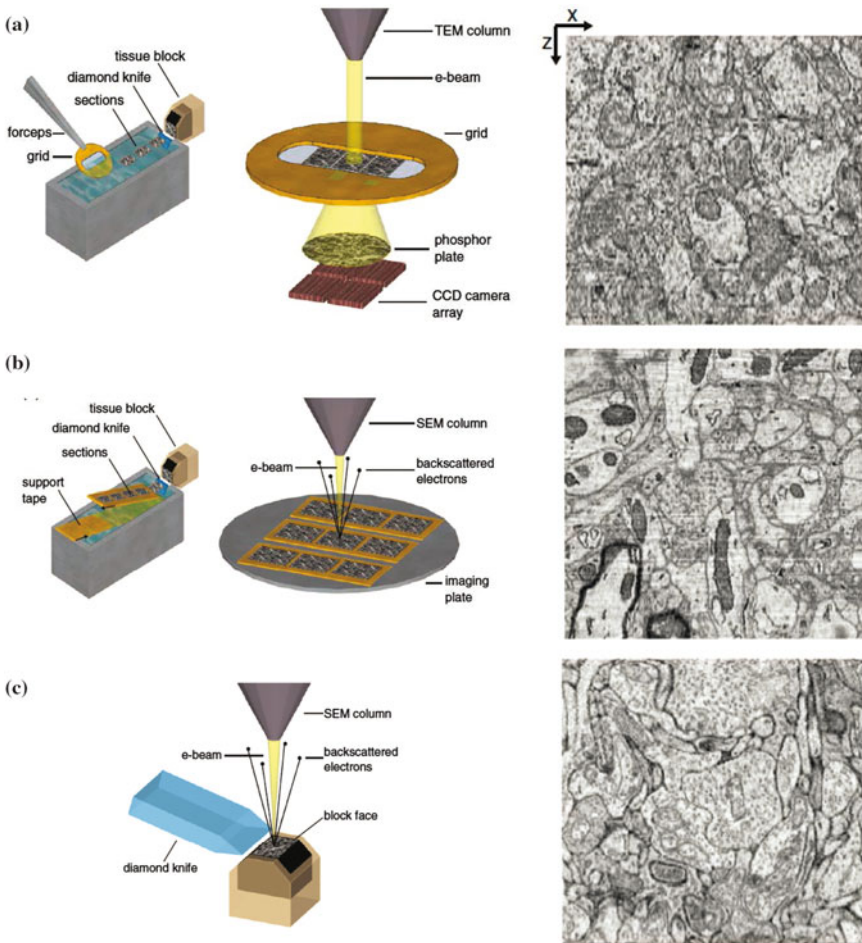


**Fig. 2.5** Automated methods to collect serial EM datasets. **a** The classical ssTEM approach was used until the advent of automated sectioning methods. One limitation of this approach is the poor  $Z$  axis resolution due to typical section thicknesses of 70–90 nm (*right panel*). **b** The automated tape-collecting ultramicrotome approach developed by K. Hayworth and J. Lichtman automates the collection of serial sections from a water boat. The automation improves the reliability of sectioning and minimal slice thicknesses of 29 nm have been reported (Kasthuri et al. 2015). The improvement in  $Z$  axis resolution is evident (*right panel*). **c** The serial block-face scanning electron microscopy (SBEM) approach developed by W. Denk. Both automated sectioning and imaging are performed within a SEM and repeatable section thicknesses down to 23 nm have been reported (Briggman et al. 2011). The improvement in  $Z$  axis resolution compared to ssTEM is evident (*right panel*). Scale bar 1  $\mu$ m. Figures reproduced from Briggman and Bock (2012)



## 2.5 The Real Bottleneck—Data Analysis

As automated EM methods have significantly eased the acquisition of high-quality 3D EM data, the size of collectable volumes has dramatically risen (Fig. 2.4a). The largest retinal volume to date spanned  $10^6 \mu\text{m}^3$ , nearly two orders of magnitude larger than previous volumes, at a voxel resolution of  $16.5 \times 16.5 \times 23 \text{ nm}^3$  (Briggman et al. 2011). Such data volumes now exceed terabytes worth of raw grayscale image data. The bottleneck is therefore now the analysis of the data. The goal is twofold: first, neuronal morphologies must be reconstructed (‘traced’) by linking together all the neurites belonging to each neuron in the volume and second, the synaptic connections between neurons must be identified. Of the two goals, the accurate reconstruction of neuronal morphologies is by far the more difficult problem. The difficulty stems from the arborized nature of most neurons. A tracing error early on in a dendritic tree can lead to the misassignment of all downstream synapses. Synapse identification, on the other hand, is a local judgement and synapse annotation errors do not typically compound.

The first serious effort to quantify error rates when reconstructing neurons was performed in an SBEM block of mouse retina (Helmstaedter et al. 2011). This study demonstrated that annotating neurons by ‘skeletonization’, delineating the midline of neurons with nodes and edges, is significantly faster than full volume reconstructions (Fig. 2.6a, b). More importantly, it was found that even experts can disagree at multiple locations when tasked with reconstructed complete morphologies. It was shown that redundant tracing of neurons by multiple independent humans can substantially reduce error rates and allow hundreds of microns of path length to be accurately traced with a small group of human annotators (Fig. 2.6c, d). This strategy was ultimately applied to reconstruct about 1000 neurons from a volume of mouse retina (Helmstaedter et al. 2013).

## 2.6 A Retinal ‘Contactome’

The first dense reconstruction all of the cells within a piece of mammalian retina was recently published (Fig. 2.7a) (Helmstaedter et al. 2013). A  $80 \times 114 \times 132 \mu\text{m}^3$  volume of mouse retina was collected using SBEM, spanning the PRL to the GCL. The analysis of this dataset yielded more than 1000 neuronal morphologies that included BCs, ACs, and GCs. One caveat of this reconstruction effort was the unconventional way in which the tissue was stained. Prior to collecting the dataset it was clear that the analysis, rather than the actual data acquisition, would be the rate-limiting step. At the time, however, it was unclear how well machine learning-based analysis algorithms (Turaga et al. 2010) would be able to automatically segment conventionally stained tissue in which, in addition to the plasma membrane, many intracellular structures are stained (such as organelles, vesicles, filaments, etc.). The retina was therefore processed with a protocol in which the surfaces of cells were

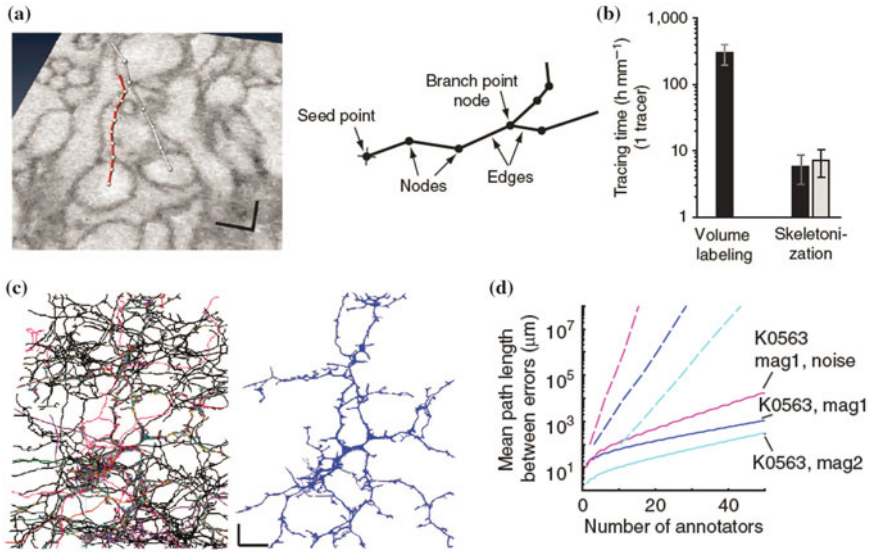


**Fig. 2.6** Annotation accuracy of mouse retina EM data. **a** Neuronal morphologies can be described by tracing the midline ‘skeletons’, consisting of a series of nodes and edges. **b** Skeletonization in the retina speeds up morphology annotation by a factor of 50 compared to 3D volume labeling. **c** The overlay of 50 human annotated skeletons of one amacrine cell demonstrates the unreliability of human annotation (*left*). A weighted consensus of the skeletons yields a more accurate representation of the cell’s morphology (*right*). **d** A calibration of the number of human annotators required to achieve a particular error rate. *Solid lines* indicate the actual performance of 50 annotators, the *dashed lines* indicate simulated error rates if the tracings were focused on locations of disagreement between annotators. Figure reproduced from Helmstaedter et al. (2011)

selectively stained and intracellular structures remained unstained (Briggman et al. 2011). The assumption was that segmentation algorithms would have an easier time delineating neurons without intracellular ‘clutter’. Qualitatively, it was far easier to follow thin neurites over hundreds of microns in such cell-surface labeled tissue compared to conventionally stained tissue. However, this approach comes with the obvious downside that vesicles remain unstained and, with them, the absolute positions of synapses are unknown.

Because the locations of synapses could not be absolutely identified, the contact area between pairs of neurons was used as a proxy for actual synaptic connectivity (Fig. 2.7b). The pairwise contact areas between all neurons thus yielded a retinal ‘contactome’ rather than a true retinal ‘connectome’ (Fig. 2.7c). Was this tradeoff worth it? Probably not, since a fully automated analysis was not ultimately error-free and multiple research groups have subsequently shown that conventionally stained tissue can be reasonably segmented to a similar degree of accuracy as the cell-surface labeled tissue (Berning et al. 2015; Pallotto 2015). In fact, the analysis of the contactome relied on a hybrid approach in which redundant

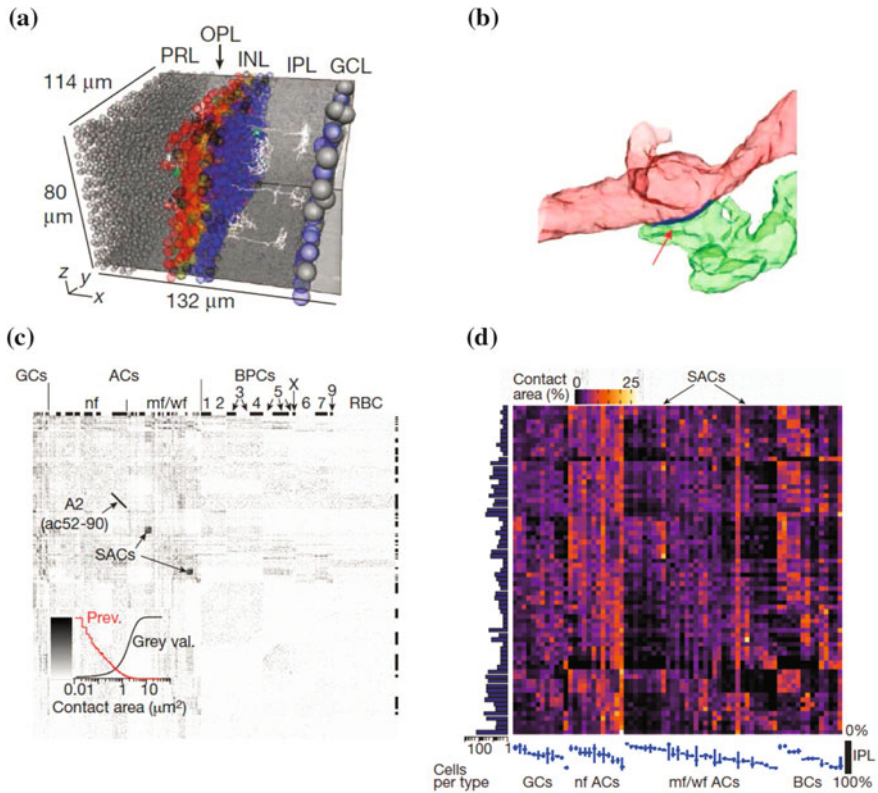


**Fig. 2.7** A contactome of the mouse retina. **a** A block of mouse retina collected by SBEM. Soma locations indicated by *spheres* and color coded by cell class: GCs large gray spheres; ACs blue; BCs red; glia yellow; horizontal cells green; photoreceptors small gray spheres. **b** An example of the contact area that was quantified between every pair of touching cells. **c** A cell-to-cell contact matrix quantifying that shared contact area between 950 neurons, sorted by class. The intensity of the *grayscale* in each matrix entry is proportional to the contact area. **d** Cells were grouped by type and the contact matrix averaged by cell type to generate a cell-type contact matrix among 71 cell types. Figures reproduced from Helmstaedter et al. (2013)

skeletonization was used to first define morphologies and automated segmentations were then used to fill out the 3D morphologies around skeletons.

Caveats aside, the contactome provided at least three crucial insights into retinal connectivity: (1) the dense reconstruction effort provided a definitive accounting of all the neurons that were in the volume, (2) any cell types that did not touch each other cannot form circuits, and (3) an analysis of shared contact area between cell types generated testable circuit hypotheses.

Quantifying how many cell types reside in the retina is perhaps the most trivial result of a dense reconstruction, but arguably one of the most crucial outcomes. The data volume was only  $80 \times 114 \mu\text{m}^2$  in the plane of the retina, precluding the reconstruction of wide-field ACs and GCs, but was sufficiently large to reconstruct

all BC types and probably the majority of AC types. Only partial GC reconstructions were obtained, but cell typing was accomplished based on IPL stratification depth. A major benefit of the retina (compared to other brain regions) is its repeating mosaic organization. Any cell typing based on morphological criterion such as stratification depth or axonal spread can therefore be verified against the mosaic formed by cells classified as a single type (with a few notable exceptions such as starburst amacrine cells that form a highly overlapping mosaic).

A novel sparse BC type was discovered (BC type X) with this approach. Given the relatively low density of this cell type, it is perhaps not surprising that this cell was missed in previous surveys (Ghosh et al. 2004). This underscores the benefit of completeness enabled by EM-based dense reconstructions. Furthermore, type 5 BCs which are morphologically difficult to separate were subtyped based on their contact patterns with specific GCs. This is an example of using connectivity to discriminate cell types and is arguably, along with gene expression profiling (Sanes and Masland 2015), one of the best ways to define distinct cell types.

Once all cell types had been identified, the shared contact area between each cell was used as a proxy for synaptic ‘weight’ in the contact matrix (Fig. 2.7c). That is, a pair of cells that share more contact area are more likely to form a stronger synaptic relationship than a pair of cells with less shared contact area. This assumption probably breaks down at some point, particularly for the special case of the ribbon synapses of bipolar cells. But the contact weight metric proved to be useful for validating existing circuit motifs and proposing new ones. Stratification between cell types has commonly been used to infer potential connectivity at the light microscopic level (Famiglietti 1992; Brown and Masland 1999). The contactome can readily rule out connectivity based on a lack of shared contact area even for cell types that extensively costratify. For example, Type 7 BCs costratify with direction selective ganglion cells (DSGCs), but were not found to share a large contact area with DSGCs. The novel BC type X was similarly found to avoid forming contacts with a GC with which it costratifies.

In addition to ruling out connectivity patterns, several circuits were proposed based on the analysis of the dominant contact areas between cell types (Fig. 2.7d). For example, the GC thought to be responsible for local-edge detection (GC type W3) (Zhang et al. 2012) was found to receive its strongest input from BC type 5R and from an ON AC, suggesting a selective role for ON feedforward inhibition onto the W3 cell. Such findings significantly narrow the number of possible cell types presynaptic to the W3 GC that need to be examined physiologically. The retinal contactome is therefore perhaps best utilized as a hypothesis generator to guide physiological studies, especially for the less well-studied circuits in the mammalian retina.

## 2.7 Correlating Retinal Structure with Function

While the retinal contactome provides an overview of possible connectivity motifs, a major goal of connectomics is to relate detailed synaptic connectivity to the function of neuronal circuits. One of the most direct demonstrations of how detailed retinal connectivity mapping can enhance the understanding of a particular computation is the analysis of the direction selective (DS) circuitry. The cell types that play a role in the computation of DS are some of the most well known and frequently studied in the mammalian retina. The uniquely shaped GABAergic starburst amacrine cells (SACs) are at the core of the circuit and their dendrites are responsible for computing direction in a radial manner relative to their central somas (Tauchi and Masland 1984; Famiglietti 1991; Euler et al. 2002). SACs violate ‘normal’ retinal mosaic principles, at least in terms of their dendritic spread. The dendrites from at least 80 or so individual SAC can be found at any given location on the retina (Ding et al. 2016). This over-representation is seemingly required by the number of postsynaptic cells with which SACs synapse—at least 7 GCs (3 subtypes of ON DSGCs and 4 subtypes of ON-OFF DSGCs) and the extensive lateral inhibition among SACs themselves.

A long-standing question regarding the computation of retinal DS was how the radial direction preference of SACs is converted to the rectilinear direction preference of DSGCs (Barlow et al. 1964; Barlow and Levick 1965). It was known from electrophysiology and synaptic pharmacology that directionally selective inhibition onto DSGCs reduces spiking along one axis and the absence of inhibition along opposing axes allow DSGCs to spike (Fried et al. 2002; Taylor and Vaney 2002). The question was how a single cell type, the SAC, could provide such directionally specific inhibition if there does not exist a dedicated SAC for each DSGC subtype?

Vaney et al. (1989) proposed a wiring principle that could explain the observed physiology. They suggested an unprecedented level of wiring specificity in which radial dendritic sectors of a single presynaptic cell selectively synapse onto different postsynaptic subtypes. In their model, the direction of presynaptic inhibitory SAC dendrites defines the null direction of a postsynaptic DSGC. How could this hypothesis be tested anatomically? Several groups analyzed proximities between SAC dendrites and DSGCs at the light microscopic level but came to differing conclusions about whether an asymmetry in SAC-to-DSGC wiring existed (Famiglietti 2002; Fried et al. 2002; Dong et al. 2004; Chen and Chiao 2008). The dense plexus of SACs makes it very difficult to accurately infer connectivity onto DSGCs with the diffraction limited optics of light microscopes. This was therefore an ideal application for modern 3D EM to test a long-standing hypothesis about retinal connectivity.

If, in fact, an asymmetric SAC-to-DSGC wiring pattern existed, the first question would be whether the pattern related to the functional properties of DSGCs. That is, to make the strongest link between structure and function, the coding properties of retinal neurons (in this case the preferred direction of DSGCs) should be

characterized in the same piece of tissue used for EM analysis. This was achieved using 2P calcium imaging of hundreds of GCs covering a  $300 \times 350 \mu\text{m}^2$  patch of mouse retina in response to moving bars (Briggman and Euler 2011; Briggman et al. 2011). The relatively unbiased imaging approach used provided the locations of dozens of ON–OFF DSGC somas. A SBEM volume was then collected from the functionally imaged area that spanned the IPL (Fig. 2.8a). Using a sparse skeletonization approach, 6 ON–OFF DSGCs and 24 SACs were reconstructed and SAC–DSGC synapses were annotated (Fig. 2.8). The analysis clearly demonstrated that the asymmetric wiring hypothesis was correct. There is a strong directional asymmetry of SAC dendrites that provide inputs to each ON–OFF DSGC subclass. Moreover, because the functional tuning curves from the reconstructed DSGCs were known, the anatomical asymmetry could be confirmed to be antiparallel to the functionally measured preferred direction of each DSGC (Fig. 2.8c). This is a clear example that mapping the structure of a circuit can actually predict its function. In other words, if one collected a new retinal EM dataset that was not functionally characterized, a key functional property of DSGCs—their preferred directions—could be with near certainty predicted solely from examining their presynaptic SAC wiring patterns.

The precision of SAC-to-DSGC connectivity is also an example of an unprecedented form of wiring specificity in the nervous system. The targeting of synapses between particular cell types is known to exist throughout the brain. The targeting of BC axons to specific sublaminae in the IPL that form synapses onto specific GCs is just one example of this. A higher degree of specificity can be found in circuits in which the axons of a given cell type (such as cortical interneurons) target particular subcellular structures (such as basal versus apical dendrites) of postsynaptic cell types (Burkhalter 2008). The SAC-to-DSGC circuit represents an even more elaborate degree of specificity in which the different dendrites of a *single* cell target different postsynaptic cell types (Fig. 2.8b).

The large SBEM volume has proven to be useful for additional studies related to the computation of DS in SAC dendrites. A massive crowd-sourced effort to reconstruct BCs in the volume revealed a spatial offset in the BC types that provide inputs to SAC dendrites (Kim et al. 2014). This spatial offset, combined with potential differences in the release kinetics of the BCs, formed the basis of a space-time wiring hypothesis that potentially contributes to the centrifugal preference of SAC dendrites.

## 2.8 Species-Dependent Differences in Retinal Wiring

While the mapping of the SAC–DSGC circuit was a definitive demonstration of the anatomical underpinnings of the DS computation, it essentially confirmed a long-standing hypothesis that was likely to be true. The broader promise of comprehensive EM-based connectomics is the ability to incorporate synaptic wiring details into novel computational models that extend our current understanding of



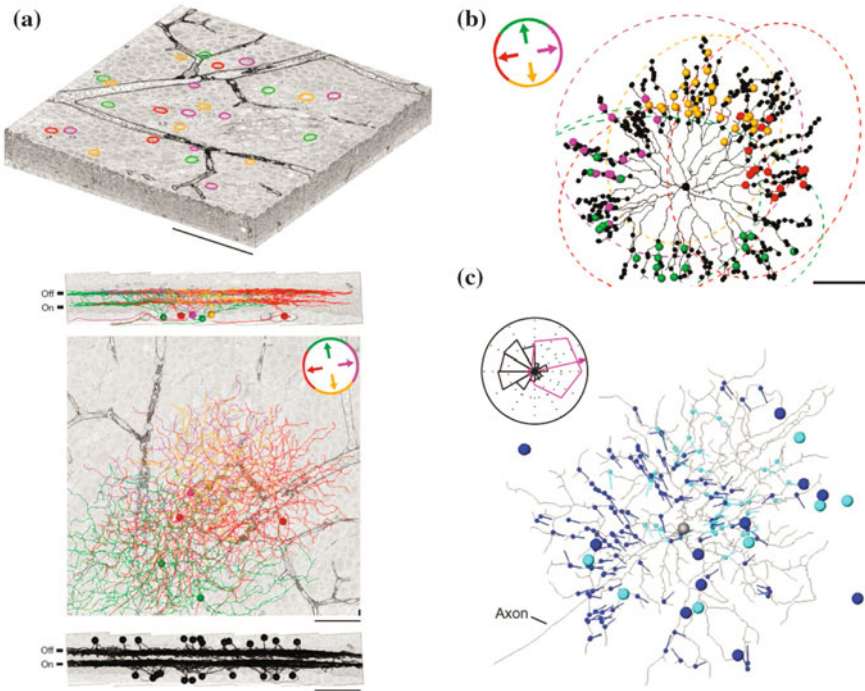


**Fig. 2.8** Wiring specificity in the direction selectivity circuit. **a** A block of mouse retina spanning the IPL collected by SBEM. GCs in the retina were functionally characterized using two-photon calcium imaging prior to EM processing. Direction selective GCs are *circled* and *color coded* by their preferred directions. The morphologies of 6 reconstructed DSGCs and 24 SACs are shown in the *lower panel*. **b** The dendrites of SACs form synapses to DSGCs with antiparallel preferred directions. Synapses color coded by the preferred direction of the postsynaptic cell (see *inset*). **c** DSGCs collect synapses from SAC dendrites oriented along their null directions. *Vectors* indicate the direction of presynaptic SAC dendrites. *Inset* The directional distribution of presynaptic SAC dendrites (*black histogram*) aligns with the null direction of a DSGC, antiparallel to the preferred direction (*magenta tuning curve*). Figure reproduced from Briggman et al. (2011)

retinal processing. A recent example of this involves the identification of species differences in the detailed wiring of the SAC-to-SAC network (Ding et al. 2016).

There are many obvious differences between the retinas of mammalian species, including the variety of high acuity regions found in different animals that are adapted to their particular environments (Linberg et al. 2001). Relatively few studies, however, have focused on species differences in the detailed synaptic wiring among cell types (Chun et al. 1993). To explore whether species differences exist in the DS circuit, a large conventionally stained SBEM dataset spanning the mouse IPL was collected that allows the positive identification of synapse locations (Fig. 2.9a). During the course of mapping the distribution of excitatory (BC synapses) and inhibitory (AC synapses) inputs onto mouse SACs, a segregation of

the inputs was found that was substantially different compared to earlier EM reconstructions of rabbit SACs (Famiglietti 1991). Excitatory BC ribbon inputs were clustered along the proximal two-thirds of SAC dendrites and were largely nonoverlapping with output synapses clustered along the outer third of the dendrites (Fig. 2.9b, c). In addition, inhibitory inputs originating primarily from neighboring SACs were located exclusively along the proximal third of SAC dendrites (Fig. 2.9c, d). By comparison, SAC-to-SAC synapses in the rabbit had been found to occur along the distal dendrites based on EM reconstruction (Famiglietti 1991) and physiological mapping of inhibitory currents (Lee and Zhou 2006).

It is important to note that the basic properties of SACs are quite similar between mouse and rabbit, including average dendritic arbor diameter, soma density, and coverage factor (Tauchi and Masland 1984; Vaney 1984; Keeley et al. 2007). Therefore, in principle, mouse SACs could have been wired together similar to rabbit SACs and vice versa. However, the most obvious difference between the two species is something much simpler than any anatomical details of the retina—their

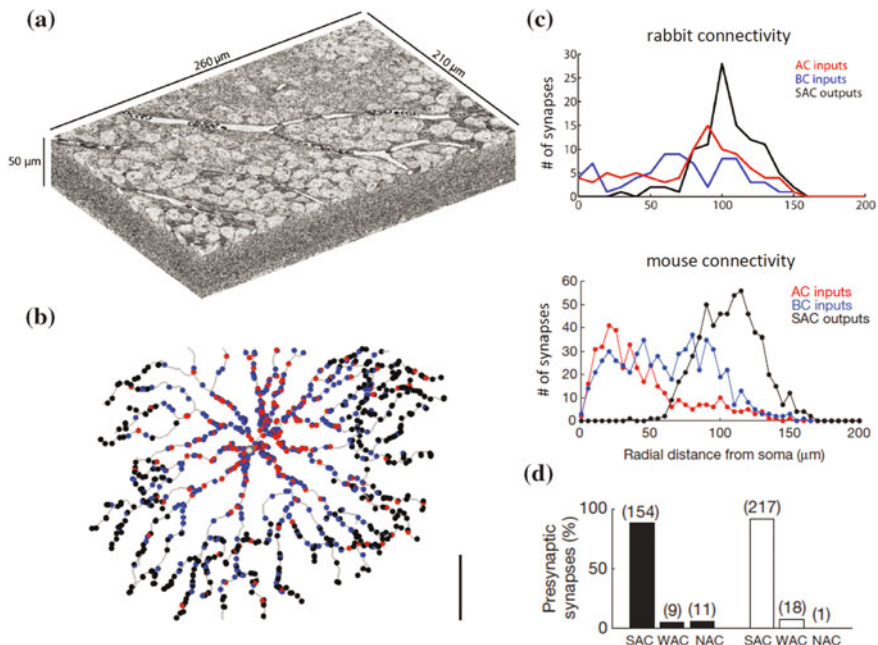


**Fig. 2.9** Species-specific wiring in the direction selectivity circuit. **a** A block of mouse retina spanning the IPL collected by SBEM. This tissue block was conventionally stained so that synapses could be positively identified. **b** A reconstruction of a SAC and annotation of excitatory (blue dots) and inhibitory (red dots) input synapses and output synapses (black dots). **c** The radial distribution of synapse types measured from rabbit SACs (upper panel) and mouse SACs (lower panel). The locus of inhibitory inputs is notably different between the two species. **d** A quantification of the types of neurons providing inhibition to mouse SACs. The majority of inputs are from neighboring SACs. Figures reproduced from Ding et al. (2016)

eye diameters. A rabbit eye is approximately 5 times larger in diameter than a mouse eye, which means an object in visual space cover a 5 times larger area on the retinas of rabbits compared to mice. This is relevant for motion processing because it also implies an object moving at constant angular velocity in visual space moves 5 times slower across the mouse retina compared to the rabbit retina. If we assume mice and rabbits experience similar objects that move at similar angular velocities during their lives, how can their retinas ensure these velocities are accurately encoded?

To explore why the SAC circuitry of the two species would be wired differently, two computational models were constructed that incorporated the detailed anatomical data derived from the EM reconstructions (Fig. 2.10a). The major difference between the two models was the separation between connected SACs. Both the rabbit and mouse models were able to generate a preference for centrifugal motion in SAC dendrites (Fig. 2.10b). However, the difference in the spatial offset of inter-SAC lateral inhibition shifted the velocity-tuning curve to prefer lower velocities in mice (Fig. 2.10c). The shift in the tuning curve was roughly by a factor of five, in remarkable agreement with the difference in eye diameters between the two species. These results imply that the rabbit and mouse retinas have adapted the SAC wiring pattern to compensate for the constraints imposed by something as simple as eye size. The detailed mapping of synaptic connectivity was essential for recognizing the difference in the first place and provided the data needed to construct anatomically constrained computational models.

## 2.9 Future of Retinal Connectomics

It has been just the few years since EM datasets large enough to encompass entire retinal circuits have become available. Even in this brief span, these datasets have been mined for multiple purposes by multiple research groups demonstrating the power of the availability of high-quality EM data to the retina research community. Both dense complete reconstructions and more limited sparse reconstructions have proven useful and both analysis approaches have identified novel circuit motifs that would have been far more difficult to identify by light microscopy. Analyzing terabyte scale EM datasets remains the rate-limiting step for generating full retinal wiring diagrams, but impressive advances in computer science promise to further decrease automated segmentation error rates in the near future. In addition to algorithm improvements, altering tissue preparation techniques, such as preserving extracellular space, can further ease automated analysis (Pallotto et al. 2015).

Will EM always be needed for connectivity mapping? Recent advances in super-resolution light microscopy have broken the diffraction limit of light and enabled proteins distributions to be mapped at nanometer scale resolutions (Rust et al. 2006). This method was recently applied to map the distribution of subunit-specific inhibitory inputs to ON-OFF DSGCs (Sigal et al. 2015). This method therefore provides multiplexed molecular information that would be

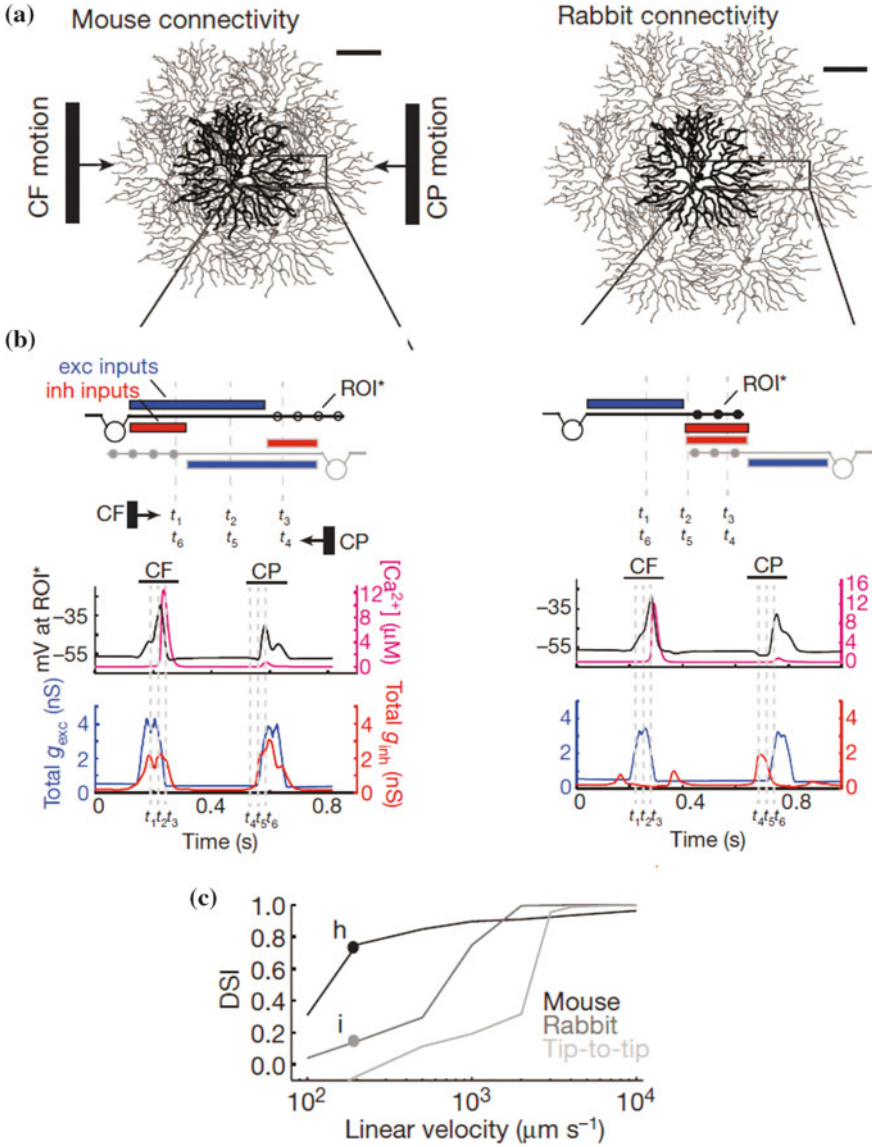


**Fig. 2.10** Functional consequences of species specific wiring. **a** Anatomically constrained network models of mouse (*left*) and rabbit (*right*) network connectivity. **b** Both network models are able to generate DS responses in which both the membrane potential and intracellular calcium concentration at dendrite tips (ROI\*) is greater for CF compared to CP motion. **c** A key difference of the two models is the velocity-tuning profiles. The models predict mouse SACs prefer slower velocities compared to rabbit SACs, consistent with the difference in eye diameter between the two species. Figures reproduced from Ding et al. (2016)

difficult to achieve with electron microscopy. Whether super-resolution methods can be extended to accurately trace fine neuronal processes in dense neuropil remains to be seen. Another recent alternative to EM is an innovative method to isotropically expand tissue before fluorescence imaging, essentially allowing proteins to be imaged at the molecular scale using diffraction limited optics (Chen et al. 2015). Again, the challenge will be to extend this technique to provide the same level of detail afforded by EM to map ultrastructure.

Now that modern automated EM methods have reached some degree of maturity, perhaps the most exciting next steps will be to compare the retinal wiring diagrams of different species in the phylogenetic tree. Most of the recent EM studies have focused on mouse, but similar large-scale efforts are underway in the rabbit retina (Anderson et al. 2011). Mapping the similarities and differences between evolutionarily distant retinas will likely provide key information to determining which parts of a circuit are essential for a computation and which are the results of species specializations.

## References

- Anderson JR, Jones BW et al (2011) Exploring the retinal connectome. *Mol Vis* 17:355–379
- Badea TC, Nathans J (2004) Quantitative analysis of neuronal morphologies in the mouse retina visualized by using a genetically directed reporter. *J Comp Neurol* 480(4):331–351
- Baden T, Berens P et al (2016) The functional diversity of retinal ganglion cells in the mouse. *Nature* 529(7586):345–350
- Barlow HB, Levick WR (1965) The mechanism of directionally selective units in rabbit's retina. *J Physiol* 178(3):477–504
- Barlow HB, Hill RM et al (1964) Retinal ganglion cells responding selectively to direction and speed of image motion in the rabbit. *J Physiol* 173:377–407
- Berning M, Boergens KM et al (2015) SegEM: efficient image analysis for high-resolution connectomics. *Neuron* 87(6):1193–1206
- Briggman KL, Bock DD (2012) Volume electron microscopy for neuronal circuit reconstruction. *Curr Opin Neurobiol* 22(1):154–161
- Briggman KL, Euler T (2011) Bulk electroporation and population calcium imaging in the adult mammalian retina. *J Neurophysiol* 105(5):2601–2609
- Briggman KL, Helmstaedter M et al (2011) Wiring specificity in the direction-selectivity circuit of the retina. *Nature* 471(7337):183–188
- Brown SP, Masland RH (1999) Costratification of a population of bipolar cells with the direction-selective circuitry of the rabbit retina. *J Comp Neurol* 408(1):97–106
- Burkhalter A (2008) Many specialists for suppressing cortical excitation. *Front Neurosci* 2(2):155–167
- Calkins DJ, Tsukamoto Y et al (1998) Microcircuitry and mosaic of a blue-yellow ganglion cell in the primate retina. *J Neurosci* 18(9):3373–3385
- Chen YC, Chiao CC (2008) Symmetric synaptic patterns between starburst amacrine cells and direction selective ganglion cells in the rabbit retina. *J Comp Neurol* 508(1):175–183
- Chen F, Tillberg PW et al (2015) Expansion microscopy. *Science* 347(6221):543
- Chun MH, Han SH et al (1993) Electron microscopic analysis of the rod pathway of the rat retina. *J Comp Neurol* 332(4):421–432
- Cohen E, Sterling P (1990) Demonstration of cell types among cone bipolar neurons of cat retina. *Philos Trans R Soc Lond B Biol Sci* 330(1258):305–321

- Coombs J, van der List D et al (2006) Morphological properties of mouse retinal ganglion cells. *Neuroscience* 140(1):123–136
- Denk W, Horstmann H (2004) Serial block-face scanning electron microscopy to reconstruct three-dimensional tissue nanostructure. *PLoS Biol* 2(11):e329
- Ding H, Smith RG et al (2016) Species-specific wiring for direction selectivity in the mammalian retina. *Nature* 535(7610):105–110
- Dong W, Sun W et al (2004) Dendritic relationship between starburst amacrine cells and direction-selective ganglion cells in the rabbit retina. *J Physiol* 556(Pt 1):11–17
- Dowling JE, Boycott BB (1966) Organization of the primate retina: electron microscopy. *Proc R Soc Lond B Biol Sci* 166(1002):80–111
- Euler T, Wässle H (1995) Immunocytochemical identification of cone bipolar cells in the rat retina. *J Comp Neurol* 361(3):461–478
- Euler T, Detwiler PB et al (2002) Directionally selective calcium signals in dendrites of starburst amacrine cells. *Nature* 418(6900):845–852
- Famiglietti EV (1991) Synaptic organization of starburst amacrine cells in rabbit retina: analysis of serial thin sections by electron microscopy and graphic reconstruction. *J Comp Neurol* 309(1):40–70
- Famiglietti EV (1992) Dendritic co-stratification of ON and ON-OFF directionally selective ganglion cells with starburst amacrine cells in rabbit retina. *J Comp Neurol* 324(3):322–335
- Famiglietti EV (2002) A structural basis for omnidirectional connections between starburst amacrine cells and directionally selective ganglion cells in rabbit retina, with associated bipolar cells. *Vis Neurosci* 19(2):145–162
- Freed MA, Sterling P (1988) The on-alpha ganglion cell of the cat retina and its presynaptic cell types. *J Neurosci* 8(7):2303–2320
- Fried SI, Munch TA et al (2002) Mechanisms and circuitry underlying directional selectivity in the retina. *Nature* 420(6914):411–414
- Gan W-B, Grutzendler J et al (2000) Multicolor “diolistic” labeling of the nervous system using lipophilic dye combinations. *Neuron* 27(2):219–225
- Ghosh KK, Bujan S et al (2004) Types of bipolar cells in the mouse retina. *J Comp Neurol* 469(1):70–82
- Gollisch T, Meister M (2010) Eye smarter than scientists believed: Neural computations in circuits of the retina. *Neuron* 65(2):150–164
- Greene MJ, Kim JS et al (2016) Analogous convergence of sustained and transient inputs in parallel on and off pathways for retinal motion computation. *Cell Rep* 14(8):1892–1900
- Helmstaedter M, Briggman KL et al (2011) High-accuracy neurite reconstruction for high-throughput neuroanatomy. *Nat Neurosci* 14(8):1081–1088
- Helmstaedter M, Briggman KL et al (2013) Connectomic reconstruction of the inner plexiform layer in the mouse retina. *Nature* 500(7461):168–174
- Huxlin KR, Goodchild AK (1997) Retinal ganglion cells in the albino rat: revised morphological classification. *J Comp Neurol* 385(2):309–323
- Jain V, Seung HS et al (2010) Machines that learn to segment images: a crucial technology for connectomics. *Curr Opin Neurobiol* 20(5):653–666
- Kasthuri N, Hayworth KJ et al (2015) Saturated reconstruction of a volume of neocortex. *Cell* 162(3):648–661
- Keeley PW, Whitney IE et al (2007) Dendritic spread and functional coverage of starburst amacrine cells. *J Comp Neurol* 505(5):539–546
- Kidd M (1962) Electron microscopy of the inner plexiform layer of the retina in the cat and the pigeon. *J Anat* 96:179–187
- Kim JS, Greene MJ et al (2014) Space-time wiring specificity supports direction selectivity in the retina. *Nature* 509(7500):331–336
- Kolb H (1970) Organization of the outer plexiform layer of the primate retina: electron microscopy of Golgi-impregnated cells. *Philos Trans R Soc Lond B Biol Sci* 258(823):261–283
- Kolb H, Nelson R et al (1981) Amacrine cells, bipolar cells and ganglion cells of the cat retina: a Golgi study. *Vision Res* 21(7):1081–1114



- Kong JH, Fish DR et al (2005) Diversity of ganglion cells in the mouse retina: unsupervised morphological classification and its limits. *J Comp Neurol* 489(3):293–310
- Lee S, Zhou ZJ (2006) The synaptic mechanism of direction selectivity in distal processes of starburst amacrine cells. *Neuron* 51(6):787–799
- Leighton SB (1981) SEM images of block faces, cut by a miniature microtome within the SEM—a technical note. *Scan Electron Microsc* 2(Pt 2):73–76
- Linberg K, Cuenca N et al (2001) Comparative anatomy of major retinal pathways in the eyes of nocturnal and diurnal mammals. *Prog Brain Res* 131:27–52
- MacNeil MA, Masland RH (1998) Extreme diversity among amacrine cells: implications for function. *Neuron* 20(5):971–982
- MacNeil MA, Heussy JK et al (1999) The shapes and numbers of amacrine cells: matching of photofilled with Golgi-stained cells in the rabbit retina and comparison with other mammalian species. *J Comp Neurol* 413(2):305–326
- Marc RE, Anderson JR et al (2014) The AII amacrine cell connectome: a dense network hub. *Front Neural Circuits* 8:104
- Masland RH (2012) The neuronal organization of the retina. *Neuron* 76(2):266–280
- McGuire BA, Stevens JK et al (1984) Microcircuitry of bipolar cells in cat retina. *J Neurosci* 4(12):2920–2938
- Pallotto M, Watkins PV et al. (2015) Extracellular space preservation aids the connectomic analysis of neural circuits. *elife* 4
- Ramón y Cajal S (1972) The structure of the retina. C. C. Thomas, Springfield
- Rockhill RL, Daly FJ et al (2002) The diversity of ganglion cells in a mammalian retina. *J Neurosci* 22(9):3831–3843
- Rust MJ, Bates M et al (2006) Sub-diffraction-limit imaging by stochastic optical reconstruction microscopy (STORM). *Nat Meth* 3(10):793–796
- Sanes JR, Masland RH (2015) The types of retinal ganglion cells: current status and implications for neuronal classification. *Annu Rev Neurosci* 38:221–246
- Schalek R, Kasthuri N et al (2011) Development of high-throughput, high-resolution 3d reconstruction of large-volume biological tissue using automated tape collection ultramicrotomy and scanning electron microscopy. *Microsc Microanal* 17(S2):966–967
- Sigal Yaron M, Speer Colenso M et al (2015) Mapping synaptic input fields of neurons with super-resolution imaging. *Cell* 163(2):493–505
- Sterling P, Freed MA et al (1988) Architecture of rod and cone circuits to the on-beta ganglion cell. *J Neurosci* 8(2):623–642
- Stevens JK, Davis TL et al (1980a) A systematic approach to reconstructing microcircuitry by electron microscopy of serial sections. *Brain Res* 2(3):265–293
- Stevens JK, McGuire BA et al (1980b) Toward a functional architecture of the retina: serial reconstruction of adjacent ganglion cells. *Science* 207(4428):317–319
- Strettoi E, Dacheux RF et al (1990) Synaptic connections of rod bipolar cells in the inner plexiform layer of the rabbit retina. *J Comp Neurol* 295(3):449–466
- Sümbül U, Song S et al. (2014) A genetic and computational approach to structurally classify neuronal types. *Nat Commun* 5:3512
- Sun W, Li N et al (2002a) Large-scale morphological survey of rat retinal ganglion cells. *Vis Neurosci* 19(4):483–493
- Sun W, Li N et al (2002b) Large-scale morphological survey of mouse retinal ganglion cells. *J Comp Neurol* 451(2):115–126
- Tauchi M, Masland RH (1984) The shape and arrangement of the cholinergic neurons in the rabbit retina. *Proc R Soc Lond B Biol Sci* 223(1230):101–119
- Taylor WR, Vaney DI (2002) Diverse synaptic mechanisms generate direction selectivity in the rabbit retina. *J Neurosci* 22(17):7712–7720
- Turaga SC, Murray JF et al (2010) Convolutional networks can learn to generate affinity graphs for image segmentation. *Neural Comput* 22(2):511–538
- Vaney DI (1984) ‘Coronate’ amacrine cells in the rabbit retina have the ‘starburst’ dendritic morphology. *Proc R Soc Lond B Biol Sci* 220(1221):501–508

- Vaney DI, Collin SP et al. (1989) Dendritic relationships between cholinergic amacrine cells and direction-selective retinal ganglion cells. *Neurobiology of the inner retina*, Springer, pp 157–168
- Volgyi B, Chheda S et al (2009) Tracer coupling patterns of the ganglion cell subtypes in the mouse retina. *J Comp Neurol* 512(5):664–687
- Wassle H, Puller C et al (2009) Cone contacts, mosaics, and territories of bipolar cells in the mouse retina. *J Neurosci* 29(1):106–117
- White JG, Southgate E et al (1986) The structure of the nervous system of the nematode *Caenorhabditis elegans*. *Philos Trans R Soc Lond B Biol Sci* 314(1165):1–340
- Zhang Y, Kim I-J et al (2012) The most numerous ganglion cell type of the mouse retina is a selective feature detector. *Proc Natl Acad Sci* 109(36):E2391–E2398

Decoding Neural Circuit Structure and Function

Cellular Dissection Using Genetic Model Organisms

Celik, A.; Wernet, M.F. (Eds.)

2017, XIII, 518 p. 92 illus., 81 illus. in color., Hardcover

ISBN: 978-3-319-57362-5